Andreas Josef Schmid*, Jonas Riest, Thomas Eckert,
Peter Lindner, Gerhard Naegele, and Walter Richtering

Comparison of the Microstructure of Stimuli Responsive Zwitterionic PNIPAM-co-Sulfobetaine Microgels with PNIPAM Microgels and Classical Hard-Sphere Systems

Abstract: In this study, we compare the experimental static structure factors of concentrated solutions of amphoteric poly(*N*-isopropylacrylamide) (PNIPAM) microgels with those of the polydisperse hard-sphere model. We use zwitterionic microgels as model systems for amphoteric microgels with an equal amount of positive and negative charges located in a defined distance. Using small angle neutron scattering (SANS), we measure the static structure factors, $S_{\mathrm{M}}(q)$, of a series of zwitterionic microgels with increasing amount of zwitterion, including a reference sample of pure PNIPAM. The experimental $S_{\mathrm{M}}(q)$ is compared with predictions based on the Percus-Yevick approximation for hard spheres. We also compare with the PNIPAM reference sample measured for zwitterionic microgels. We find no significant influence of the zwitterionic comonomer on the effective pair potential. The PNIPAM and the zwitterionic microgels can be described by the hard-sphere model for smaller volume fractions $\phi_T \lesssim 0.4$ only.

Keywords: Microgel, PNIPAM, Zwitterion, Structure factor.

DOI 10.1515/zpch-2014-0559
Received June 30, 2014; accepted September 11, 2014

***Corresponding author: Andreas Josef Schmid,** Institute of Physical Chemistry, RWTH Aachen University, Landoltweg 2, 52056 Aachen, Germany, e-mail: aschmid@pc.rwth-aachen.de
Thomas Eckert, Walter Richtering: Institute of Physical Chemistry, RWTH Aachen University, Landoltweg 2, 52056 Aachen, Germany
Jonas Riest, Gerhard Naegele: Institute of Complex Systems (ICS-3), Research Centre Jülich, 52425 Jülich, Germany
Peter Lindner: Institut Laue Langevin (ILL), Avenue des Martyrs, 38000 Grenoble, France

1 Introduction

One class of colloidal particles, which during the past years gained a lot of interest in soft matter science and in industrial applications such as printing [1] or pharmaceutics [2], are microgels. These are intramolecularly crosslinked, spherical polymer networks swollen in a good solvent. They combine the properties of macroscopic gels and of colloidal suspensions [3].

Poly(styrene) (PS) or poly(methylmethacrylate) (PMMA) microgels are often regarded as nearly hard-sphere-like particles with a purely repulsive short-range potential. They have been used to investigate the crystallisation behaviour and the glass transition in concentrated suspensions [4–6]. The introduction of a short-ranged attraction can be achieved by adding a short-chained, linear polymer to the microgel suspension. This leads at first to the melting of the colloidal glass, and with increasing strength of the attraction to a "re-entrant" glass transition [7]. Bartsch et al. also found a hard-sphere-like behaviour of PS microgels well below the colloid glass transition by a mode-coupling theory analysis of dynamic light scattering (DLS) data [8]. However, close to the glass transition, the behaviour differs from the hard-sphere model. Very low crosslink densities result in softness of the particles. Shape fluctuations and deformations allow thus the particles to escape from their cages. Recent theoretical-experimental studies [9–11] account for the softness of the particle through the usage of an appropriate soft interaction potential. One possible choice is the non-diverging, bounded Hertz potential which describes the energy penalty of the deformation of two homogeneous spheres. The potential is useful for microgels of low crosslinking density and/or small size, which result in low deformation energies. However, for microgels of radius $R \gtrsim 50$ nm, the energy cost for significant deformations is very high ($\sim 10^4 k_B T$) resulting in an effective hard-sphere (HS) behaviour [12].

Poly(*N*-isopropylacrylmide) (PNIPAM) microgels show an even more complex colloidal behaviour due to their thermoresponsiveness in water. They exhibit a volume phase transition (VPT) at 32 °C in aqueous solution [13–15]. Stieger et al. showed with small angle neutron scattering (SANS) that PNIPAM microgels in the swollen state have a different structure compared to homogeneous spheres. This internal particle structure changes with temperature [16]. Below the volume phase transition temperature (VPTT), PNIPAM microgels can be described as "fuzzy spheres", and above the VPTT as a homogeneous sphere. In a different study, Stieger et al. could also show that the static structure factor, $S(q)$, of swollen PNIPAM microgels can be successfully described by the hard-sphere model despite of their inhomogeneous structure [17]. Eckert et al. found a similar behaviour of $S(q)$ for low volume fractions of microgels [3]. While in [3] the collective dif-

fusion coefficient and the hydrodynamic functions are not describable by the HS model already for low volume fractions, an improved theoretical analysis by Riest et al. [12] shows that the hard-sphere model is able to capture the dynamics of microgels in the full fluid-like regime, provided that an appropriate model for the internal particle hydrodynamics is used.

Introducing weak acidic [18–21] or basic [22–24] comonomers into a PNIPAM microgel leads to multisensitive microgels (temperature, pH, ionic strength). A pH-induced swelling of the microgel is caused by the osmotic pressure of the counterions [25]. PNIPAM-co-acrylic acid (AAc) microgels at pH < pK_a, where Coulomb repulsion is minimized, have been used as model system to investigate the influence of weak attractive and soft repulsive interactions on the particle concentration indicating that H-bonding might be relevant [26–28]. Mohanty et al. used the same system in a deprotonated state at intermediate pH to study the phase behaviour [29]. They showed that the interaction potential is a screened Coulomb potential. They further found a transition from a liquid to a face centred cubic (FCC) crystalline structure above 0.03 wt %. For higher concentrated samples, an additional body centred cubic (BCC) crystalline structure occurred. Furthermore, their experimental phase diagram fits to the theoretical predictions for an ionic microgel by Gottwald et al. [30], with a re-entrant disordered state at very high concentrations. Huang et al. investigated a cationic microgel system of PNIPAM-co-allylamine and found the same phase transitions from liquid to crystalline to a colloidal glass [31]. Recently, Holmqvist et al. published a combined theoretical-experimental study of the structure and dynamics of negatively charged PNIPAM-co-AAc microgels [32]. They show that the swelling of the particles depends on the number density of particles, in addition to the dependence on pH and salinity.

Amphoteric microgels contain both acidic and basic comonomers, and are therefore interesting systems due to the presence of opposite charges [33–35]. Amphoteric microgels swell in acidic and basic pH, and are collapsed at intermediate pH, which is the so-called zwitterionic regime. The simplest way to synthesize amphoteric microgels is to use a zwitterionic comonomer, e.g. sulfobetaine [35]. Betaines carry an identical number of opposite charges in a well-defined distance, which makes zwitterionic microgels ideal model systems of amphoteric microgels. One might expect, that the presence of opposite charges in the microgel network influences the interactions between the particles.

In the present study, we investigate the equilibrium microstructure of amphoteric microgels in concentrated, salt free suspensions. Using SANS, we measure the angular dependent scattering intensity, $I(q)$, of a series of zwitterionic microgels over a broad concentration range (0.2 wt % to 6 wt %). We determine the experimentally measurable static structure factor, $S_M(q)$, and compare it with pre-

dictions based on the hard-sphere model with polydispersity included. We have used microgels with various amounts of sulfobetaine (0 mol % to 3 mol % in the monomer feed) to study the influence of the amount of opposite charges on the microstructure.

2 Experimental part

Chemicals: *N*-isopropylacrylamide (NIPAM, 99%) was purchased from Acros Organics, [3-(Methacryloylamino)propyl]diemthyl(3-sulfopropyl) ammonium hydroxide inner salt (sulfobetaine, 96%) from Sigma Aldrich. *N,N'*-methylenebisacrylamide (BIS, +99%, Alfa Aesar) was used as a crosslinker. Potassium persulfate (KPS, 99%) and sodium dodecylsulfate (SDS, 98%) were purchased from Merck. Methacryloxyethyl thiocarbamoyl rhodamine B (MRB, Polysciences) was used as fluorescence dye. Deuterated water (D_2O, 99.9%) was bought from Deutero. Bidistilled milli-Q-water was used for the synthesis.

Synthesis: Microgels were synthesized by free radical precipitation polymerization [36]. The reaction was performed in 1 L of water in a 2 L-three neck flask equipped with a mechanical stirrer, reflux condenser and a nitrogen inlet. 1 L of water was degassed with nitrogen. 80 mL of degassed water were taken and kept. Monomers, crosslinker, fluorescence dye (0.03 mmol) and SDS were added to the reaction vessel, whereupon the weighting vessels were rinsed with 30 ml of the taken water (structural formulas can be seen in Figure 1). The solution was heated up to 75 °C oilbath temperature and flushed with nitrogen for at least 1 h. KPS was

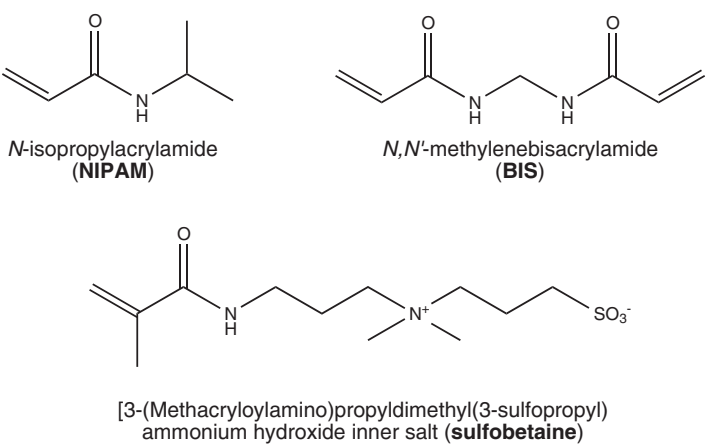

Figure 1: Structural formulas of the monomers NIPAM, sulfobetaine and the crosslinker BIS used to synthesize zwitterionic microgels.

Table 1: Composition of the reaction mixtures during the synthesis of the zwitterionic microgels.

	N0		N1		N2		N3	
	m [g]	n [mmol]	m [g]	n [mmol]	m [g]	n [mmol]	m [g]	n [mmol]
NIPAM	22.6326	200	22.4054	198	22.1785	196	21.9531	194
sulfobetaine	0	0	0.5853	2	1.1698	4	1.7549	6
BIS	1.5421	10	1.5418	10	1.5424	10	1.5419	10
SDS	0.5769	2	0.5768	2	0.5773	2	0.5774	2
KPS	0.5411	2	0.5413	2	0.5409	2	0.5412	2
MRB	0.0226	0.03	0.0230	0.03	0.0234	0.03	0.0234	0.03

dissolved in 50 mL of the taken water and added to the solution with a syringe. The reaction was performed for 6 h under stirring at 250 rpm under nitrogen flow. After 6 h the oil bath was removed, the nitrogen flow was turned off, and the solution was allowed to cool down to room temperature over night and filtrated over glass wool. The solution was cleaned by four cycles of centrifugation. Between each centrifugation step the supernatant was replaced by water and the solution was redispersed. After the fourth step of centrifugation, the microgel solution was freeze-dried.

Small Angle Neutron Scattering (SANS): A 6 wt % stock solution in D_2O was prepared by adding the solvent to freeze-dried microgel powder. For complete dispersion, samples were equilibrated on a roll mixer, slightly centrifuged and mixed at temperatures far below and slightly above the VPTT. More dilute

samples were prepared by dilution of the stock solution and equilibration on the roll mixer. Experiments were performed at the instrument D11 at the Institut Laue-Langevin (ILL) in Grenoble, France. A wavelength of $\lambda = 6$ Å with a polydispersity $\Delta\lambda/\lambda$ of 9% was used.

Samples were measured at three sample-detector distances of 1.2 m, 8 m and 39 m to cover the entire available q-range of the instrument. The scattering intensity was detected on a ^{3}He gas detector (CERCA) with a detection area of 96×96 cm^2 and a pixel size of 7.5×7.5 mm^2. Narrow Hellma quartz glass cells (type 110-QS) with 1 mm sample thickness were used. The incoherent scattering of water was measured as secondary calibration standard at 8 m sample-detector distance. All data were corrected for transmission, empty cell scattering and background scattering to receive absolute values for the differential cross section.

Zwitterionic microgels were measured in a copper sample changer at 20 °C. The sample temperature was measured inside a cell filled with water by an external thermometer and adjusted by an external thermostat. Measurements at 39 m sample-detector distance had to be scaled by a factor of 1.5 so that they overlap with the data from 8 m sample-detector distance, as calibration with water is not possible at this sample-detector distance. Sample N0 was measured at 24 ± 2 °C without additional temperature control by means of thermostat. This corresponds to an uncertainty in the particle size of about 3%, as estimated from the DLS measurement of the particle hydrodynamic radius in the temperature interval 22 °C–26 °C. Thus, the particle size in the measurement with sample N0 is practically constant.

Dynamic light scattering (DLS): DLS samples were prepared by dispersing freeze-dried microgels in D_2O. To avoid multiple scattering, the samples were highly diluted. The samples were filtrated through a 0.8 or 1 µm filter to avoid dust contamination into cylindrical cells (Hellma, 540.110-QS, 75 mm high, 10 mm outer diameter, 8 mm inner diameter). All measurements were performed on an ALV setup equipped with a 633 nm HeNe laser (JDS Uniphase, 35 mW), a goniometer (ALV, CGS-8F), digital hardware correlator (ALV 5000), two avalanche photo diodes (Perkin Elmer, SPCM-CD2969), a light scattering electronics unit (ALV, LSE-5003), an external programmable thermostat (Julabo F32) and an index-match-bath filled with toluene. All measurements were recorded pseudo cross-correlated. Temperature was measured inside the index-match-bath and regarded as sample temperature.

All samples were measured at scattering angles of 30–140° in steps of 10° for 60 s. Temperature dependent measurements were performed in the range of 10–50 °C in 2 °C steps. Heating and cooling curves were recorded and match perfectly.

The apparent diffusion coefficient, D_{app}, was extracted using the method of cumulants as proposed by Koppel [37]. At each temperature, the apparent mutual or collective diffusion coefficient, D, was determined by extrapolation of D_{app} to zero angle [38]. The translational Stokes-Einstein equation [39] was used to deduce an effective hydrodynamic radius, R_h, from the diffusion coefficient measurement at high dilution where the concentration dependence of D_{app} can be neglected.

3 Theory and data analysis

In small angle neutron scattering, the experimentally measured scattering intensity $I(q)$ is directly related to the differential cross section $\mathrm{d}\sigma(q)/\mathrm{d}\Omega$. The differential cross section is independent of transmission and defined as the number of scattered neutrons into an element of solid angle $\mathrm{d}\Omega$ into the direction of the scattering vector $\vec{q}$. The magnitude, q, of the scattering vector is

$$q = \frac{4\pi}{\lambda} \sin\left(\frac{\theta}{2}\right) \tag{1}$$

where λ is the neutron wavelength, and θ the scattering angle. The differential scattering cross section corrected for incoherent flat background at large momentum transfer for polydisperse, spherical colloidal particles of the same material can be expressed for dominant single scattering as

$$\frac{\mathrm{d}\sigma(q)}{\mathrm{d}\Omega} \propto I(q) \propto n_T \overline{f^2}(q) S_M(q) \tag{2}$$

where n_T is the total number density of particles in the scattering volume [40]. Here, $S_M(q)$ is the so called measurable static structure factor, and $\overline{f^2}(q)$ is the second moment of the particle scattering amplitudes taken with respect to the size distribution function. The overline characterizes an average with respect to this distribution function. The measurable structure factor describes the scattering amplitude averaged particle-particle correlations resulting from the interference of scattered neutron waves. Note that for a polydisperse system, $S_M(q)$ is not a purely statistical mechanical quantity but is influenced also by the intra-particle scattering properties. Thus, $S_M(q \to 0)$ is in general different from the isothermal osmotic compressibility.

For non-dilute suspensions, $S_M(q)$ is obtained experimentally by dividing the scaled measured intensity, $I(q)$, of the non-dilute sample of number density, n_T, by the scaled intensity, $I_0(q)$, of a reference sample at a sufficiently lower density

n_T^0 where particle correlations can be neglected (i.e., where $S_M^0(q) \cong 1$). Thus,

$$\frac{I(q)/n_T}{I_0(q)/n_T^0} = \frac{\overline{f^2(q)}S_M(q)}{\overline{f^2(q)}S_M^0(q)} \approx S_M(q). \tag{3}$$

It has been assumed here that the particle scattering amplitudes and the size distribution do not change with concentration.

The scattering amplitude, $f(q)$, characterizes the scattering properties of a single spherical microgel particle. It arises from the interference of intraparticle scattering sites and is related to the measurable form factor $P_M(q)$. For a polydisperse (multicomponent) system, the latter is given by

$$P_M(q) = \frac{\overline{f^2(q)}}{\overline{f^2(q=0)}} \tag{4}$$

and normalized such that $P_M(q=0) = 1$.

Although microgels exhibit spherical geometry on average, the particle scattering amplitudes of PNIPAM microgels differ from that of homogeneously scattering spheres. The different reaction kinetics of the crosslinker BIS and NIPAM lead to an inhomogeneous crosslink density inside the microgel, resulting in a fuzzy surface.

In the present work, we use a scattering amplitude model by Stieger et al. [16] depicted in Figure 2. In this model, the scattering amplitude of a crosslinked microgel is related to that of a core-shell-like particle with core radius R and a shell of width $2\sigma_{surf}$. The amplitude is obtained from the convolution of the radial scattering length distribution of a homogeneous sphere of radius R_{box} with a Gaussian function of constant width $1/\sigma_{surf}$, with the latter accounting for the non-homogeneous cross-linking density. Explicitly,

$$f(qR) = R^3 \frac{j_1(qR)}{qR} \exp\left(-\frac{(q\sigma_{surf})^2}{2}\right), \tag{5}$$

where $R = R_{box} + 2\sigma_{surf}$, and $j_1(x)$ is the first order spherical Bessel function. The total radius in the scattering amplitude model is

$$R_{HC} = R + 2\sigma_{surf}. \tag{6}$$

Here the subscript HC (hard core) denotes that this radius is used as the particle excluded volume radius in our polydisperse correlation functions calculations.

The chemically produced microgels have a certain distribution of inner radii R, globally characterized by the mean radius $\overline{R}$, and the relative standard deviation, s_R, defined as

$$s_R = \frac{\left[\overline{R^2} - \overline{R}^2\right]^{\frac{1}{2}}}{\overline{R}} = [t+1]^{-\frac{1}{2}}, \tag{7}$$

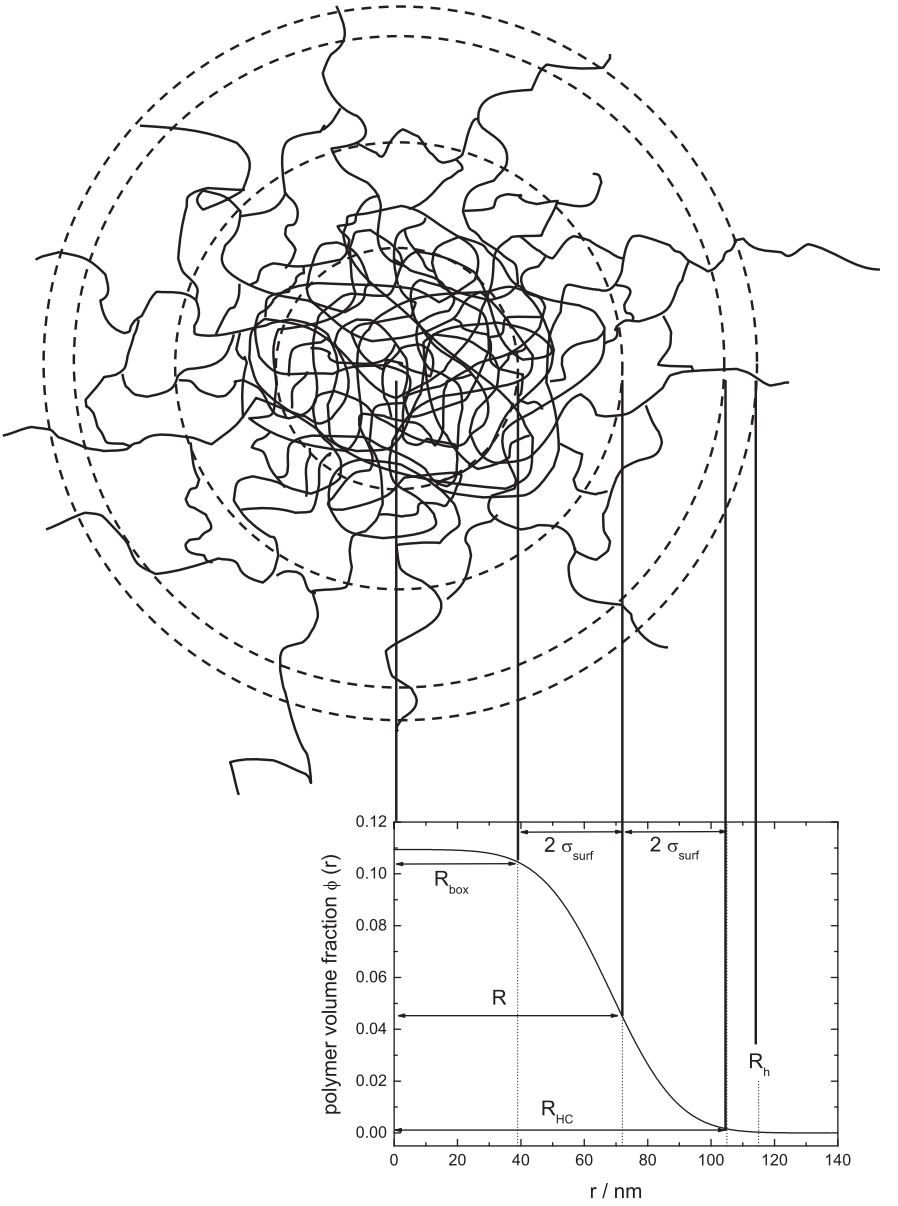

Figure 2: Schematics of the scattering amplitude model taken from Stieger et al. [16] For more details see Stieger et al. [16].

where t is a non-dimensional width parameter. For the size distribution function $p_s(R;\overline{R};s_R)$, we use the unimodal and skew-symmetric Schulz distribution function given by (see, e.g. [41])

$$p_s\left(R;\overline{R};s_R\right) = \left[\frac{t+1}{\overline{R}}\right]^{t+1} \frac{R^t}{\Gamma(t+1)} \exp\left[-\frac{t+1}{\overline{R}}R\right], \ (t>0) \tag{8}$$

with moments

$$\overline{R^n} = \int_0^\infty dR\ R^n\ p_s\left(R;\overline{R};s_R\right) = \frac{(n+t)!}{t!(t+1)^n}\overline{R}^n, \tag{9}$$

for $n \in \{0,1,\ldots\}$.

For smaller polydispersities, the Schulz distribution can be well approximated by a Gaussian distribution function centred at $R = \overline{R}$. In accordance with experimental observations, only the particle core of radius R and thus R_{HC} is treated as polydisperse, whereas the shell width $2\sigma_{\mathrm{surf}}$ is kept constant.

For calculating the measurable static structure factor in Equation (2) for a size polydisperse system, we employ a m-component histogrammatic approximation of the continuous Schulz distribution (see [40]) so that

$$S_{\mathrm{M}}(q) = \frac{1}{\overline{f^2}(q)} \sum_{\alpha,\beta=1}^{m} (x_\alpha x_\beta)^{\frac{1}{2}} f_\alpha(q)\ f_\beta(q)\ S_{\alpha\beta}(q). \tag{10}$$

Here, x_α are the molar fractions of components $\alpha \in \{1,2,\ldots,m\}$ with respective excluded volume radii R_α. The values of the histogrammatic distribution $\{x_\alpha, R_\alpha\}$ are determined by enforcing the equality of the first $2m$ moments of the histogrammatic representation of the Schulz distribution (see [40] for details).

Therefore,

$$\overline{f^n}(q) = \int_0^\infty dR\ p_s\left(R;\overline{R};s_R\right) f^n(q,R) = \sum_{\alpha=1}^{m} x_\alpha f^n(qR_\alpha) \tag{11}$$

with $\sum_{\alpha=1}^{m} x_\alpha = 1$.

The $m(m+1)/2$ partial structure factors are related to the partial total correlation functions, $h_{\alpha\beta}(r)$, by

$$S_{\alpha\beta}(q) = \delta_{\alpha\beta} + 4\pi n_{\mathrm{T}}(x_\alpha x_\beta)^{\frac{1}{2}} \int_0^\infty dr\ r^2\ h_{\alpha\beta}(r)\ \frac{\sin(qr)}{qr}. \tag{12}$$

For size polydispersities $s_R < 0.3$, it is sufficiently accurate to use a $m = 4$ component histogrammatic representation.

To calculate the $S_{\alpha\beta}(q)$'s for a mixture of hard spheres of radius distribution $\{R_\alpha\}$, we employ the analytic Percus–Yevick solution for the Laplace transform,

$$\tilde{H}_{\alpha\beta}(s) = \int_0^\infty dr\ r\ h_{\alpha\beta}(r)\ e^{-sr} \tag{13}$$

of $rh_{\alpha\beta}(r)$ provided by Blum and Hoye [42]. Using this solution, the $S_{\alpha\beta}(q)$'s are obtained in a straightforward way from the imaginary part as

$$S_{\alpha\beta}(q) = \delta_{\alpha\beta} + \frac{4\pi(n_\alpha n_\beta)^{\frac{1}{2}}}{q} Im\left[H_{\alpha\beta}(s = iq)\right]. \tag{14}$$

The total volume fraction, ϕ_T, of the polydisperse hard-sphere system is given by the third moment of the excluded volume radii distribution as

$$\phi_T = \frac{4\pi}{3} n_T \overline{R^3_{HC}}. \tag{15}$$

The polydisperse Percus–Yevick hard-sphere solution is known to be decently good for volume fractions $\phi_T \lesssim 0.3$ and lower polydispersities $s_R \lesssim 0.15$. At any rate, it is only applicable to fluid-like systems. For $\phi_T \geq 0.3$ where the (multicomponent) Percus–Yevick (PY) approximation becomes less accurate, the so-called decoupling approximation for $S_M(q)$ can be used for analytic simplicity [40, 43]. This approximation allows for the usage of the Verlet–Weis corrected Percus Yevick solution for monodisperse hard spheres, with the size polydispersity accounted for in the scattering amplitudes only. Thus, the $h_{\alpha\beta}(r)$'s are approximated by the total correlation function, $h_{id}(r)$, of an ideally monodisperse system of same volume fraction ϕ_T and total number density n_T as those of the actual polydisperse system. Explicitly,

$$h_{\alpha\beta}(r) \approx h_{id}(r; \phi_T, R^*_{HC}) \tag{16}$$

where

$$R^*_{HC} = \left(\overline{R^3_{HC}}\right)^{\frac{1}{3}} = \overline{R_{HC}}\ \left[1 + \mathcal{O}\left(s_R^2\right)\right]. \tag{17}$$

The measurable structure factor, $S_D(q)$, in the decoupling approximation is then given by

$$S_M(q) \approx S_D(q) = [1 - X(q)] + X(q)\ S_{id}\left(q; \phi_T; R^*_{HC}\right) \tag{18}$$

where $S_{id}(q; \phi_T; R^*_{HC})$ is the static structure factor of the ideally monodisperse system [40].

The function $X(q)$ in the decoupling approximation incorporates the scattering amplitude polydispersity and reads [40]

$$X(q) = \frac{\left[\overline{f}(q)\right]^2}{\overline{f^2}(q)}. \tag{19}$$

Note that $0 \leq X(q) \leq 1$.

As shown in [44], the principal peak height of the Verlet–Weis (VW) corrected hard-sphere structure factor at wavenumber position q_m is up to $\phi_T \lesssim 0.54$ given to a good approximation by

$$S_{id}(q_m) \approx 1 + 0.644\ \phi_T\ g_{id}^{CS}(2R_{HC}^*; \phi_T), \tag{20}$$

where $g_{id}^{CS}(2R_{HC}^*; \phi_T)$ is the Carnahan Starling contact value of the hard-sphere radial distribution function. According to MD simulation results by Rintoul and Torquato [45, 46], $g_{id}^{CS}(2R_{HC}^*; \phi_T)$ applies also to the metastable fluid branch of the hard-sphere phase diagram for volume fractions up to the melting point value 0.54.

A comparison of the decoupling approximation result with the polydisperse Percus Yevick solution for $S_M(q)$ is presented in Figure 3. For illustrative purposes, the calculations have been performed for a system of homogeneously scattering spheres of mean radius $\overline{R}$ and polydispersity $s_R = 0.105$ at volume fraction $\phi_T = 0.25$. Polydispersity leads to a smearing out of the maxima and minima, and to a reduction of the principal peak height compared to the monodisperse system characterized by $S_{id}(q)$ [41]. The decoupling approximation overestimates the measurable structure factor at low q values, and it has a more pronounced first minimum than the polydisperse PY solution. Yet, the principal peak form of $S_M(q)$ is nicely reproduced in the decoupling approximation, for the considered lower s_R values.

We mention that an analytic extension of the polydisperse PY solution for $\tilde{H}_{\alpha\beta}(s)$, valid for higher volume fractions, has been provided by Santos et al. [47].

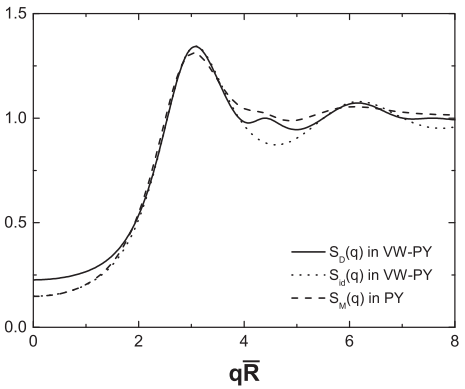

Figure 3: Comparison of the decoupling approximation $S_D(q)$ (solid line) of $S_M(q)$ with the polydisperse PY solution for homogeneous scattering spheres of mean radius $\overline{R}$, polydispersity $s_R = 0.105$ and volume fraction $\phi_T = 0.25$ (dashed line). Further shown is the VW-PY structure factor $S_{id}(q)$ of an ideally monodispers system (dotted line, see Equation (18)).

For simplicity, however, and since the considered s_R values are rather small, we restrict ourselves to the usage of the decoupling approximation with VW-PY input for $S_{\mathrm{id}}(q)$.

4 Results and discussion

We have synthesized a series of zwitterionic microgels with increasing amount of sulfobetaine. The amount of sulfobetaine was varied from 0 mol %, which is the reference system PNIPAM, to 3 mol % in the monomer feed. The crosslinking ratio of 1 : 20, which is the molar ratio of crosslinker to monomer, was kept constant for all samples to achieve a similar volume swelling ratio S for all samples. The surfactant SDS was used to stabilize the particle surface during the synthesis, and to produce small particles which can be analysed by small angle scattering techniques. The monomer feeds of the microgels are summarized in Table 1. Detailed information about the physicochemical properties of these particles in dilute solution and the role of sulfobetaine during the synthesis in the presence of SDS was obtained in a different work by Schmid et al. [48] and will be published elsewhere.

First, the angular dependent scattering intensity, $I(q)$, was measured in the dilute regime for all samples in D_2O well below the VPTT (Figure 4). The zwitterionic microgels were measured at 20 °C, and the PNIPAM sample at 24 ± 2 °C. The scattering curves were fitted according to the model of Stieger et al. [16]. The fits represent the data over the entire q-range very well. The slight deviations in the high-q region can be due to small errors in the treatment of incoherent scattering. The important fit parameters are summarized in Table 2.

The mean excluded-volume radius $\overline{R}_{\mathrm{HC}}$ was calculated from these fitting parameters using Equation (6).

Secondly, a series with increasing mass fractions in heavy water in the range of 1 wt %–6 wt % was prepared for all samples. The scattering curves of the different mass fractions were measured and normalized to the mass fraction c according to Equation (3). We neglect the difference in density between microgel and solvent so that the particle density n_{T} is determined by the mass fraction. Figure 5 shows the normalized angular dependent scattering intensity, $I(q)/n_{\mathrm{T}}$, at 20 °C and at 24 ± 2 °C in the case of sample N0. All scattering curves overlap in the high-q-regime, indicating only minor errors in the mass fractions within the series. The most pronounced effect on $I(q)$ with increasing mass fraction occurs at low q. The scattering intensity, $I(q)$, is reduced by approximately two orders of magnitude for all samples in the small q limit.

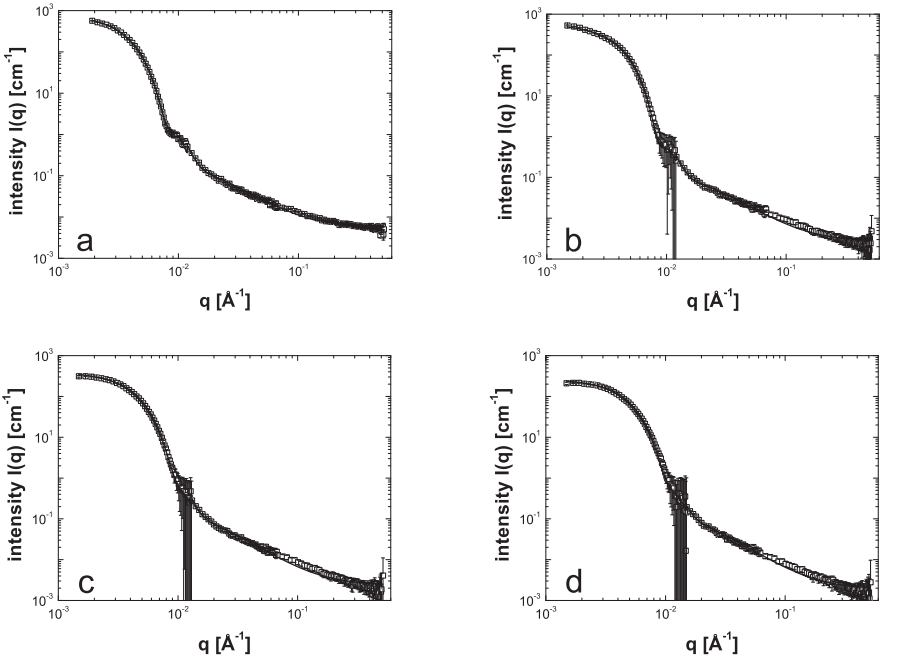

Figure 4: Scattering curves of samples N0 (a), N1 (b), N2 (c) and N3 (d) in D_2O at 20 °C (sample N0 was measured at 24 °C ± 2 °C). The concentration is about 0.2 wt %. Solid lines represent fits according to the form factor model of Stieger et al. [16] given in Equation (5). Large error bars in the intermediate q-range are due to the low statistics at the border of the detector.

Table 2: Parameters obtained from fitting the scattering curves for samples N0–N4 in D_2O at 20 °C (sample N0 was measured at 24 ± 2 °C) according to the form factor model of Stieger et al. [16] given in Equation (5). Note that $\bar{R}_{HC} = \bar{R} + 2\sigma_{surf}$. For completeness, we also list values for the effective hydrodynamic radius, R_h, determined using low-q DLS.

sample	$\overline{R}$ [nm]	σ_{surf} [nm]	s_R [%]	$\overline{R}_{HC}$ [nm]	R_h [nm]	R_{HC}/R_h
N0	54.2	13.1	13.5	80.4	92[1]	0.874
N1	50.7	14.1	10.5	78.9	90	0.877
N2	42.6	12.7	17.5	68.0	81	0.840
N3	39.9	10.3	17.0	60.5	78	0.776

[1] R_h in D_2O at 24 °C.

This indicates an increased correlation between the particles with increasing mass fraction, as indicated by smaller $S_M(q)$ values. For sample N0, the scattering intensity decreases continuously in going from 0.2 wt % to a concentration of 5 wt %, and increases then again. The zwitterionic microgels, however, show all

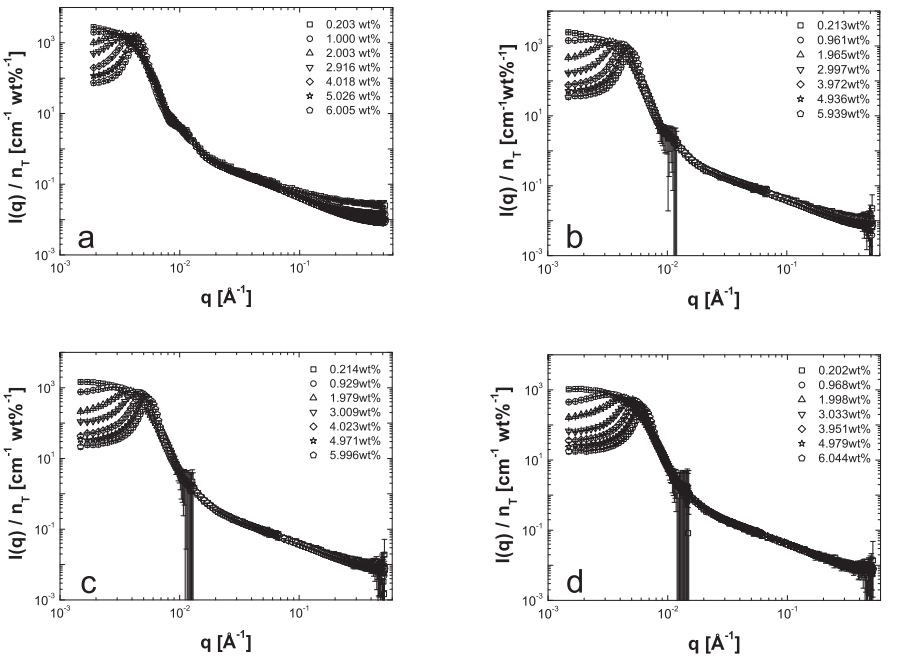

Figure 5: Normalized scattering curves of samples N0 (a), N1 (b), N2 (c) and N3 (d) in D_2O at 20 °C (sample N0 was measured at 24 ± 2 °C) at various concentrations as indicated.

a similar behaviour, with the scattering intensity decreasing monotonically in going from 0.2 wt % to 6 wt %.

Next, the experimental static structure factor, $S_M(q)$, has been deduced using Equation (3), with results presented in Figure 6. The structure factor peak position, q_m, is shifted to higher q-values with increasing concentration, for all considered samples.

This is indicative of a lowering inter-particle distance with increasing mass fraction, since for lower polydispersities the centre-to-centre distance, d, of neighbouring particles scales inversely with the structure factor peak position as

$$d \sim \frac{2\pi}{q_m}. \tag{21}$$

The experimental peak height, $S_M(q_m)$, determined from $I(q)$ has the same trend in its concentration dependence as $I(q \to 0)$.

We fit the experimental $S_M(q)$ using the decoupling approximation approach in conjunction with the Verlet–Weis approximation. The only fitting parameter is the total volume fraction in Equation (15). The values for s_R and $\overline{R}_{HC}$ are deter-

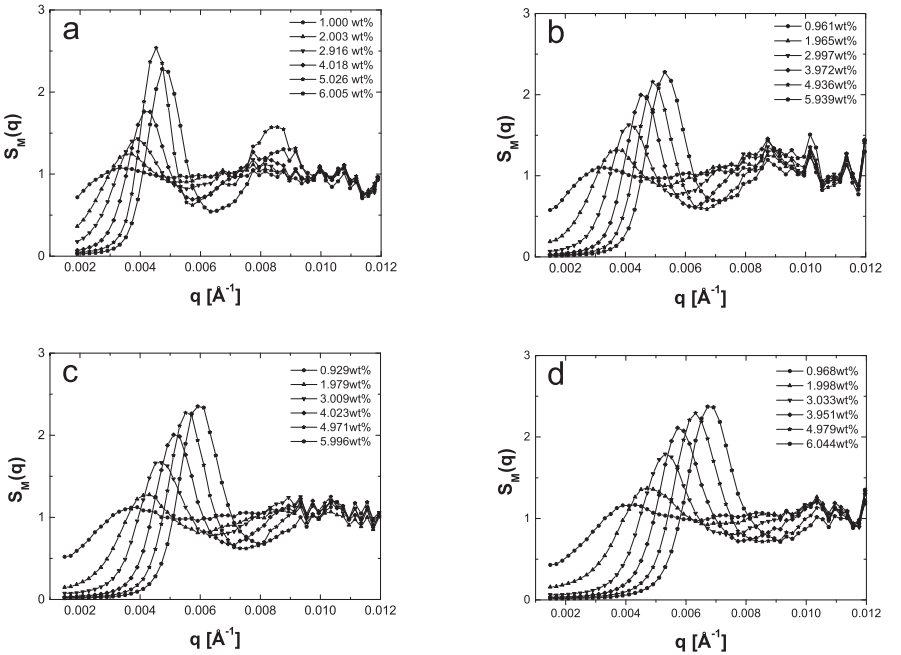

Figure 6: Measurable static structure factors, $S_M(q)$, of samples N0 (a), N1 (b), N2 (c) and N3 (d) in D_2O at 20 °C (sample N0 was measured at 24 ± 2 °C) for different concentrations as indicated. The lines are guides to the eye.

mined from the low concentration fits of $\overline{f^2}(q)$ and are kept constant in the $S_M(q)$ fits. See Table 2 for their values. Results are presented in Figure 7.

For values $\phi_T \leq 0.4$, the theoretical fits based on the (polydisperse) hard-sphere model describe the experimental structure factor data for all samples quite well.

At higher volume fractions $\phi_T > 0.4$, theoretical and experimental data deviate significantly from each other for all considered samples. The experimental principal peak positions, q_m, are shifted to higher q-values compared to the theoretical predictions. This indicates a lower centre-to-centre distance d (see Equation (21)). The PNIPAM based microgels can achieve this either by deswelling and thus lowering the particle size, or by overlapping. The latter mechanism appears reasonable at high volume fractions owing to the inhomogeneous structure and lower polymer density on the particle surface. The former mechanism leads to a visible change in the scattering curve, in particular regarding the locations of the local minima. It should be noticed here that the form of $I(q)$ is changed not

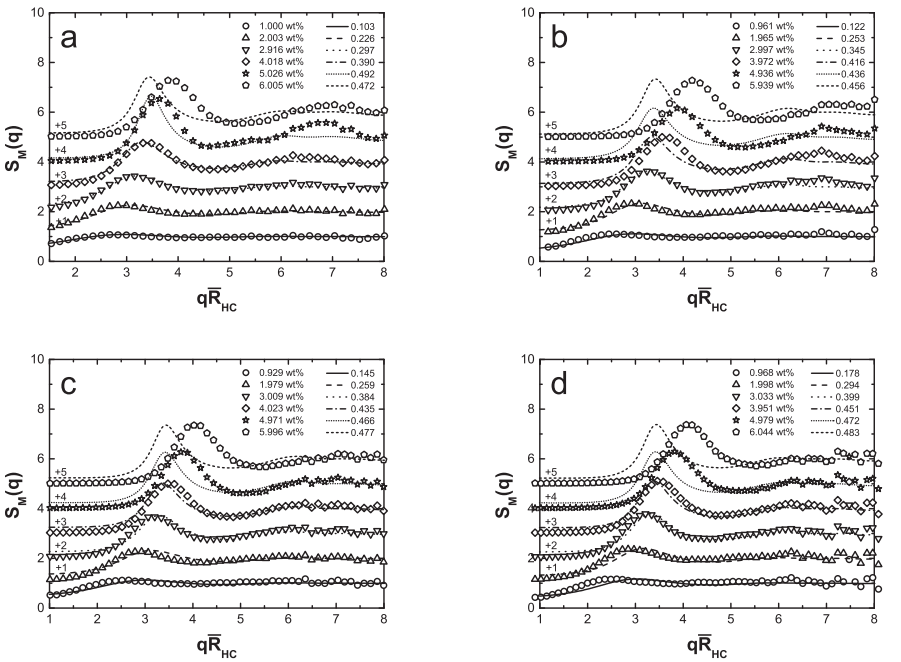

Figure 7: Measurable static structure factors, $S_M(q)$, of samples N0 (a), N1 (b), N2 (c) and N3 in D_2O at 20 °C (sample N0 was measured at 24 ± 2 °C) at various concentrations as indicated. The lines are theoretical structure factors based on the hard-sphere pair potential and the decoupling approximation combined with the PY-VW solution for $S_{id}(q)$.

only through the changing form factor at high concentrations, but also through the changing $S_M(q)$.

The temperature responsiveness, and by this the particle sizes of PNIPAM microgels in aqueous solution, are altered by the solvent quality. The solvent quality is determined by the strength of the hydrogen bonds between water molecules and NIPAM. These should not depend on the particle concentration, which renders a shrinking of the particles as rather unlikely. Contrast variation experiments of a mixture of deuterated and protonated PNIPAM microgels can provide information on the particle form factor in concentrated solutions, and on the particle shrinking or overlapping. This will be the topic of a future investigation.

There is no visible influence of the zwitterionic comonomer, since the hard-sphere structure factors describe all scattering data equally well for the four considered systems. We conclude thus that at low volume fractions, the hard-sphere potential suitably describes the (effective) pair interactions between pure PNIPAM (N0) microgels, and between the zwitterionic microgels.

It is also noticeable that for all samples, $S_M(q \to 0)$ decreases monotonically with increasing n_T. A significant increase of $S_M(q)$ in the low-q-regime with increasing n_T is an indicator for the existence of (effective) attractive forces between the particles. For an example relevant in this context, Baxter [49] uses an attractive surface adhesion potential in addition to the hard-sphere potential, leading to a $S_M(q)$ which increases with concentration in the low-q-regime.

On first sight, one might expect an attractive contribution to the pair potential due to the incorporation of the zwitterionic comonomer. However, the purely repulsive hard-sphere potential is sufficient to describe the static structure factors of the zwitterionic microgels even up to $\phi_T \approx 0.4$. At very high volume fractions, however, where the microgels can overlap, the experimental data do not show evidence for attractive forces between the zwitterionic microgels. This absence of attraction can be due to two possible mechanisms: First, the rather low amount of incorporated charges is not sufficient to cause attraction. Secondly, the formation of internal salt between the sulfonate headgroup and the quaternary ammonium group of sulfobetaine is more favourable than intermolecular salt formation.

5 Conclusion

In this study, we have investigated the influence of opposite charges in a PNIPAM microgel network on the equilibrium microstructure. We have used a series of zwitterionic microgels with increasing amount of zwitterionic comonomer, and determined the measurable static structure factors using SANS. We compared the experimental data with a pure PNIPAM reference sample, and with the classical hard-sphere system predictions. The measurable static structure factors can be well described by the hard-sphere model up to $\phi_T \approx 0.4$. We find no significant influence of the zwitterionic comonomer on the effective pair potential, for the $S_M(q)$ of all zwitterionic microgels is also well described by the hard-sphere model up to $\phi_T \approx 0.4$. At higher volume fractions, the experimental data of all samples deviate significantly from the hard-sphere model. In this high concentration range, the microgels are likely to overlap or deswell. We conclude that in concentrated solutions, zwitterionic microgels with equal amounts of charges behave, similarly to pure PNIPAM, as effective hard spheres for $\phi_T \leq 0.4$.

Acknowledgement: The authors thank the Deutsche Forschungsgemeinschaft DFG for funding within the SFB 985 "Functional microgels and microgel systems". J. Riest is grateful for the support by the IHRS BioSoft.

References

1. N. Sasa and T. Yamaoka, Adv. Mater. **6** (1994) 417.
2. V. C. Lopez, S. L. Raghavan, and M. J. Snowden, React. Funct. Polym. **58** (2004) 175.
3. T. Eckert and W. Richtering, J. Chem. Phys. **129** (2008) 124902.
4. P. N. Pusey and W. van Megen, Nature **320** (1986) 340.
5. P. Pusey, W. van Megen, P. Bartlett, B. Ackerson, J. Rarity, and S. Underwood, Phys. Rev. Lett. **63** (1989) 2753.
6. T. Eckert and E. Bartsch, J. Phys.-Condens. Mat. **16** (2004) S4937.
7. T. Eckert and E. Bartsch, Phys. Rev. Lett. **89** (2002) 125701.
8. E. Bartsch, V. Frenz, J. Baschnagel, W. Schärtl, and H. Sillescu, J. Chem. Phys. **106** (1997) 3743.
9. J. Riest, P. Mohanty, P. Schurtenberger, and C. N. Likos, Z. Phys. Chem. **226** (2012) 711.
10. D. Paloli, P. S. Mohanty, J. J. Crassous, E. Zaccarelli, and P. Schurtenberger, Soft Matter **9** (2013) 3000.
11. P. S. Mohanty, D. Paloli, J. J. Crassous, E. Zaccarelli, and P. Schurtenberger, J. Chem. Phys. **140** (2014).
12. J. Riest, T. Eckert, W. Richtering, and G. Nägele, to be published.
13. R. H. Pelton and P. Chibante, Colloid. Surface. **20** (1986) 247.
14. R. Pelton, Adv. Colloid Interfac. **85** (2000) 1.
15. H. G. Schild, Prog. Polym. Sci. **17** (1992) 163.
16. M. Stieger, W. Richtering, J. S. Pedersen, and P. Lindner, J. Chem. Phys. **120** (2004) 6197.
17. M. Stieger, J. S. Pedersen, P. Lindner, and W. Richtering, Langmuir **20** (2004) 7283.
18. M. J. Snowden, B. Z. Chowdhry, B. Vincent, and G. E. Morris, J. Chem. Soc. Faraday T. Trans. **92** (1996) 5013.
19. C. Johansson, J. Gernandt, M. Bradley, B. Vincent, and P. Hansson, J. Colloid Interf. Sci. **347** (2010) 241.
20. C. D. Jones and L. A. Lyon, Macromolecules **36** (2003) 1988.
21. J. Kleinen and W. Richtering, Macromolecules **41** (2008) 1785.
22. X. Hu, Z. Tong, and L. A. Lyon, Colloid Polym. Sci. **289** (2010) 333.
23. V. T. Pinkrah, M. J. Snowden, J. C. Mitchell, J. Seidel, B. Z. Chowdhry, and G. R. Fern, Langmuir **19** (2003) 585.
24. V. J. Cornelius, M. J. Snowden, J. Silver, and G. R. Fern, React. Funct. Polym. **58** (2004) 165.
25. H. Ni, H. Kawaguchi, and T. Endo, Colloid Polym. Sci. **285** (2007) 819.
26. M. Keerl, V. Smirnovas, R. Winter, and W. Richtering, Angew. Chem. Int. Edit. **47** (2008) 338.
27. Z. Meng, J. K. Cho, S. Debord, V. Breedveld, and L. A. Lyon, J. Phys. Chem. B **111** (2007) 6992.
28. A. N. S. John, V. Breedveld and, L. A. Lyon, J. Phys. Chem. B **111** (2007) 7796.
29. P. S. Mohanty and W. Richtering, J. Phys. Chem. B **112** (2008) 14692.
30. D. Gottwald, C. N. Likos, G. Kahl, and H. Löwen, Phys. Rev. Lett. **92** (2004) 068301.
31. G. Huang and Z. Hu, Macromolecules **40** (2007) 3749.
32. P. Holmqvist, P. S. Mohanty, G. Nägele, P. Schurtenberger, and M. Heinen, Phys. Rev. Lett. **109** (2012) 048302.
33. S. Schachschal, A. Balaceanu, C. Melian, D. E. Demco, T. Eckert, W. Richtering, and A. Pich, Macromolecules **43** (2010) 4331.

34. M. Das and E. Kumacheva, Colloid Polym. Sci. **284** (2006) 1073.
35. M. Das, N. Sanson, and E. Kumacheva, Chem. Mater. **20** (2008) 7157.
36. A. Pich and W. Richtering, Adv. Polym. Sci. **234** (2010) 1.
37. D. E. Koppel, J. Chem. Phys. **57** (2003) 4814.
38. W. Burchard and W. Richtering, Prog. Coll. Pol. Sci. **80** (1989) 151.
39. A. Einstein, Ann. Phys. **322** (1905) 549.
40. G. Nägele, Phys. Rep. **272** (1996) 215.
41. E. Canessa, M. J. Grimson, and M. Silbert, Solid State Commun. **64** (1987) 145.
42. L. Blum and J. S. Høye, J. Phys. Chem. **81** (1977) 1311.
43. J. S. Pedersen, Adv. Colloid Interfac. **70** (1997) 171.
44. A. J. Banchio and G. Nägele, J. Chem. Phys. **128** (2008) 104903.
45. M. D. Rintoul and S. Torquato, J. Chem. Phys. **105** (1996) 9258.
46. M. Rintoul and S. Torquato, Phys. Rev. Lett. **77** (1996) 4198.
47. S. B. Yuste, A. Santos, and M. López de Haro, J. Chem. Phys. **108** (1998) 3683.
48. A. J. Schmid, R. Schröder, T. Eckert, A. Radulescu, A. Pich, and W. Richtering, to be published.
49. R. J. Baxter, J. Chem. Phys. **49** (1968) 2770.